Synsint Research Group

Available online at www.synsint.com

Synthesis and Sintering

ISSN 2564-0186 (Print), **ISSN** 2564-0194 (Online)

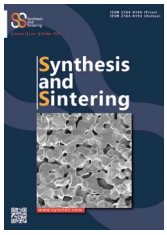

Research article

Influence of TiN addition on densification behavior and mechanical properties of ZrB_2 ceramics

Alain Shima [a,*], **Masoud Kazemi** [b]

[a] *Department of Aeronautical Engineering, University of Kyrenia, Kyrenia, Cyprus*
[b] *Ceramic Department, Materials and Energy Research Center (MERC), Karaj, Iran*

A B S T R A C T

In the present work, densification behavior and mechanical features (fracture toughness and Vickers hardness) of undoped and TiN-doped ZrB_2 ceramic materials, hot-pressed at 1800 °C under 15 MPa for 1 h, were studied. The addition of only 5 wt% TiN into ZrB_2 has resulted in an increase in its relative density from 83% to 90%. Removal of oxide contaminations like B_2O_3 via chemical reactions with TiN and new secondary phases formation such as ZrN, h-BN, and $(Zr,Ti)B_2$ solid solutions were approved employing crystalline phase analysis and microstructural studies. Improvement of densification and restriction of grain growth caused enhancement of mechanical characteristics. The measured values of Vickers hardness and fracture toughness are ameliorated from 7.8 GPa and 1.5 $MPa.m^{1/2}$ to 14.1 GPa and 3.8 $MPa.m^{1/2}$, respectively.

KEYWORDS

ZrB_2
TiN
Densification
Sinterability
Mechanical properties

OPEN ACCESS

1. Introduction

As a member of ultra-high temperature ceramic (UHTC), zirconium diboride has gained the researchers' interest owing to its high melting temperature and excellent accumulation of features including low thermal expansion coefficient, chemical inertness, electrical conductivity, and high hardness [1–3]. Its relatively low density along with aforesaid characteristics has made ZrB_2 an appropriate candidate for potential usages commonly in re-entry vehicles and aerospace industries. However, the applicability of this material has been challenged because of poor sinterability caused by its strong covalent bonds and low self-diffusion coefficient [1, 4, 5]. Hence, applying high pressures and elevated temperatures is necessary to obtain a fully dense ZrB_2 sample, which encourages the growth of grains and results in a significant decline in fracture toughness. To overcome such problems, several research works have suggested the selection of suitable consolidation techniques and/or activating the toughening and sintering mechanisms utilizing the addition of additives [6–8]. Among spark plasma sintering (SPS), pressureless sintering (PS), reactive hot pressing (RHP), and hot pressing (HP) [9, 10], as the sintering techniques for the fabrication of UHTCs, the first one is a newly developed route that utilizes direct current pulsing and external mechanical pressure to densify the materials synchronously [11–13].

According to the role of additives/ reinforcements, both metals and non-metals can be utilized as the sintering aid to prevail over mentioned shortcomings of ZrB_2 and improve its properties. Additives like Mo [14], V [15], Cr, Fe [16], Al [17], Ni [18], Nb [19], and Ti [20] are the typical metallic component used in ZrB_2-based ceramics that can form liquid phase during the densification process and ameliorate the sinterability.

Several non-metallic sintering additives incorporated to ZrB_2 materials to remove the oxide dirt from the particles' surface through chemical reactions and improve the densification are carbides, carbon allotropes, boride, and nitrides. Aside from borides and carbides, the influence of refractory nitrides HfN [21], ZrN [22], Si_3N_4 [23, 24], BN [25–30], TiN [31], and AlN [32, 33] on the mechanical properties, the densification promotion, and microstructural evolution of sintered UHTCs have newly been investigated as sintering aids or reinforcements in

* Corresponding author. *E-mail address:* k20190648@std.kyrenia.edu.tr (A. Shima)
Received 4 December 2022; Received in revised form 29 March 2023; Accepted 30 March 2023.

https://doi.org/10.53063/synsint.2023.31133

Table 1. Characteristics of as-purchased powders.

Material	Purity (%)	Particle size (µm)	Supplier	Role
ZrB_2	99.5	≤1.5	Xuzhou Hongwu Nano-material Company, China	Matrix
TiN	99.5	≤1	Xuzhou Hongwu Nano-material Company, China	Additive

ZrB_2-based materials. Sinterability and densification of ZrB_2-SiC composites are enhanced by adding the appropriate amount of AlN leading to liquid phase formation, which fills the porosities and voids in microstructure [32, 33]. Surface oxide contaminations on the ZrB_2 particles are purged by adding BN additive through the chemical reaction between BN and ZrO_2 and subsequently thermal shock resistance, sinterability, machinability, and flexural strength are improved [25, 26]. Fully dense ZrB_2–SiC ceramic composites are hot pressed by adding 3 vol% HfN or 4.5 vol% ZrN owing to liquid phase formation [21, 22]. Another nitride component used as a sintering aid to promote sinterability and develop the microstructure of ZrB_2 is Si_3N_4, which can form nano-platelet boron nitride and borosilicate amorphous phase at the grain boundaries [24]. This nitride also affects the mechanical behavior and sinterability of TiB_2 manufactured by hot-pressing because of cleaning the surface oxide contaminations leading to the formation of SiO_2, BN, and TiN [34, 35]. However, in addition to mentioned synthesized phases, TiC and B_4C were also formed as the in-situ secondary phases in the SPSed TiB_2–SiC ceramic composite [36, 37]. The introduction of enough content of AlN encourages the sintering process and densification of hot-pressed TiB_2 due to obliterating the surface oxide dirties such as TiO_2 [38].

Using TiN additive is reported in TiB_2-based ceramic, resulting in the fabrication of a nearly fully dense sample [31]. The introduction of TiN in TiB_2–SiC composite resulted in the fabrication of fully dense material, including TiC, nano-layered BN, B_4C, and TiSi via the spark plasma sintering [39]. (Zr,Ti)B_2–(Zr,Ti)N ceramic composite is fabricated due to the in-situ synthesis and penetration of ZrN and TiB_2 as the result of TiN addition to the ZrB_2 ceramic and their chemical reactions during the spark plasma sintering [40]. The Appearance of in-situ synthesized h-BN, the solid solution of (Zr,Ti)B_2, and ZrN as well as ZrO_2 was proved in TiN-doped ZrB_2–SiC leading to mechanical properties improvement [41].

In the present work, the pure ZrB_2 and the ZrB_2-5 wt% TiN ceramic materials were fabricated utilizing the hot-pressing method at 1800 °C under an external pressure of 15 MPa for the holding time of 60 min to peruse the influence of TiN sintering additive on the sinterability, microstructure, and mechanical characteristics of ZrB_2 UHTC.

2. Experimental procedure

2.1. Materials and methods

Commercially as-purchased ZrB_2 and TiN powder were employed as the initial materials in the present work. The more important characteristics of these initial powders have been illustrated in Table 1. 5 wt% TiN was weighted and added into a certain amount of ZrB_2 to produce a ZT powder mixture. After that, the specified amount of ZrB_2 (Z) powder and ZT powder mixture as the precursors were homogenized employing an ultrasonic bath for 20 min in the ethanol. Then, the obtained slurries were ball-mixed for 1 h at 80 rpm. Next, blended slurries were dried up by holding them in a rotary oven (HMS 14, Tebazma, Iran) at 110 °C for 180 min. The desiccated powder mixtures were ground using a pestle and an agate pounder, then sieved to prevent their agglomeration (100-mesh). Eventually, each prepared powder mixture was poured into a graphite mold with an inner radius of 1.5 cm covered by flexible graphite foil to decrease the probability of chemical reaction among the die and powders. The sintering process was carried out at 1800 °C for 60 min under a load of 15 MPa in vacuum condition using hot pressing apparatus (Shenyang Weitai Science & Technology Development Co., Ltd., Shenyang China).

2.2. Characterization

The bulk density of as-sintered specimens was measured utilizing the Archimedes method with distilled water as the immersing medium. Theoretical density was evaluated by rule-of-mixture. In order to attain the relative densities, the ratio of the measured bulk densities to the calculated theoretical ones was estimated. Field-emission scanning electron microscopy (FE-SEM: Mira3 Tescan, Czech Republic) and energy-dispersive X-ray spectroscopy (EDS) were simultaneously utilized to investigate the microstructure and chemical composition of as-sintered specimens. Identification of crystalline phases was performed using X-ray diffraction (XRD: Philips PW1730). Indents were created on the polished surface of as-sintered samples by applying a force of 49 N for 15 s and a mean Vickers hardness (H_v) was determined. Indentation fracture toughness (K_{IC}) of samples was diagnosed from the measurement of mean cracks length, based on the Anstis equation [42]:

$$K_{IC} = 0.016\left(\frac{P}{C^{3/2}}\right)\left(\frac{E}{H_v}\right)^{1/2} \quad (1)$$

where C, E, H_v, and P are the average half-length of the radial cracks, Youngs' modulus (specified by the rule of mixtures), Vickers hardness, and applied indentation load, respectively.

3. Results and discussion

The microstructure of the polished surface of as-sintered Z and ZT samples is displayed in Fig. 1. These micrographs display the good harmony of microstructure and the obtained relative densities of Z and ZT. Relative densities of 83% and 90% were achieved for Z and ZT samples after hot pressing at 1800 °C under 15 MPa for 1 h. As it is clear in Fig. 1a, some porosity remains in the microstructure of Z samples showing that the sintering condition is not appropriate to manufacture the fully-dense monolithic ZrB_2. As seen in Fig .1, using small content of TiN (5 wt%) in ZrB_2 as a sintering additive has led to porosities elimination, secondary in-situ phase formation, and relative density improvement. But some pores and agglomerated areas are still present in the microstructure of the ZT specimen. This agglomerated area seems to prevent more densification owing to entrapping the porosities. In addition to the silver main phase distributed through the microstructure (ZrB_2), several newly formed phases with various colors including dim gray, black, and light gray phases can be seen. Such observations indicate the chemical reactions between the initial powders that occurred during the hot-pressing process.

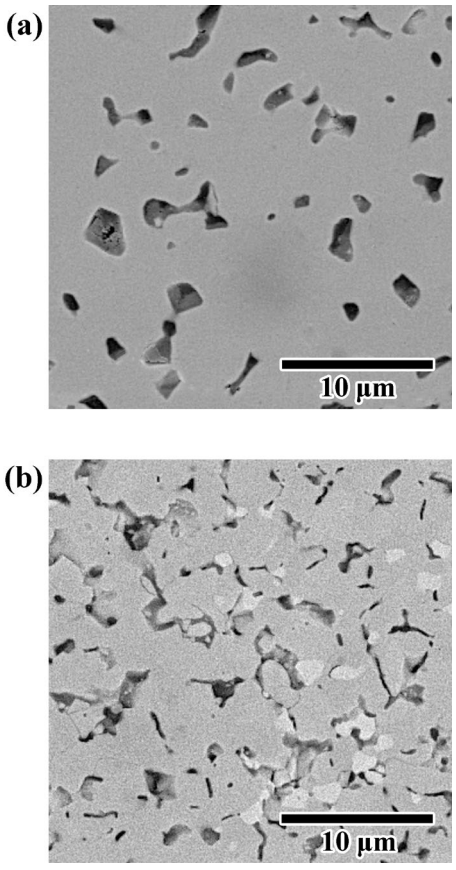

Fig. 1. Polished surfaces of as-sintered a) Z and b) ZT specimens.

Higher magnification of the polished surface of the as-sintered ZT sample containing agglomerated phase along with corresponding EDS elemental mapping is exhibited in Fig. 2. From Fig. 2, the concentration of zirconium and boron in their elemental map shows that the matrix is ZrB_2. On one hand, in the agglomerated area, the concentration of mentioned elements decreases. On the other hand, the presence of titanium in all regions shows the intention of this element to diffuse from the Ti-rich area to other grains. In this situation, the solid solution formation of $(Zr,Ti)B_2$ is possible. Such observation has been carried out in the ZrB_2-TiN manufactured by the spark plasma sintering method [43]. Some dim gray areas in the microstructure can be seen that may be ZrO_2 according to the concentration of oxygen and zirconium. Since ZrB_2 powder as a non-oxide material, naturally tends to observe and react with the oxygen, some oxides such as ZrO_2 can exist on the surface of its particles. Therefore, this phase can remain and be detected. Therefore, this phase can be left over from raw materials or formed as a result of chemical reactions among initial phases during the sintering procedure. It is clear from Fig. 1b and Fig. 2, some light gray phases are uniformly distributed in the microstructure, which can be guessed that such phases are related to ZrN due to their light color and the corresponding elemental map. It is worth saying; it is hard to detect some light elements such as nitrogen and boron in the corresponding EDS elemental maps. The concentration of nitrogen and boron in the black area shows the probability of BN formation as the in-situ synthesized phase. In addition to the black phases, there are other phases that seem to be ZrB_2 or $(Zr,Ti)B_2$ solid solution inside the orange circle. The synthesis of $(Zr,Ti)B_2$ solid solution is also reported in spark plasma sintered ZrB_2-SiC-TiN and ZrB_2-TiN ceramics [43, 44].

Fig. 3 displays the secondary electron mode FE-SEM image of the

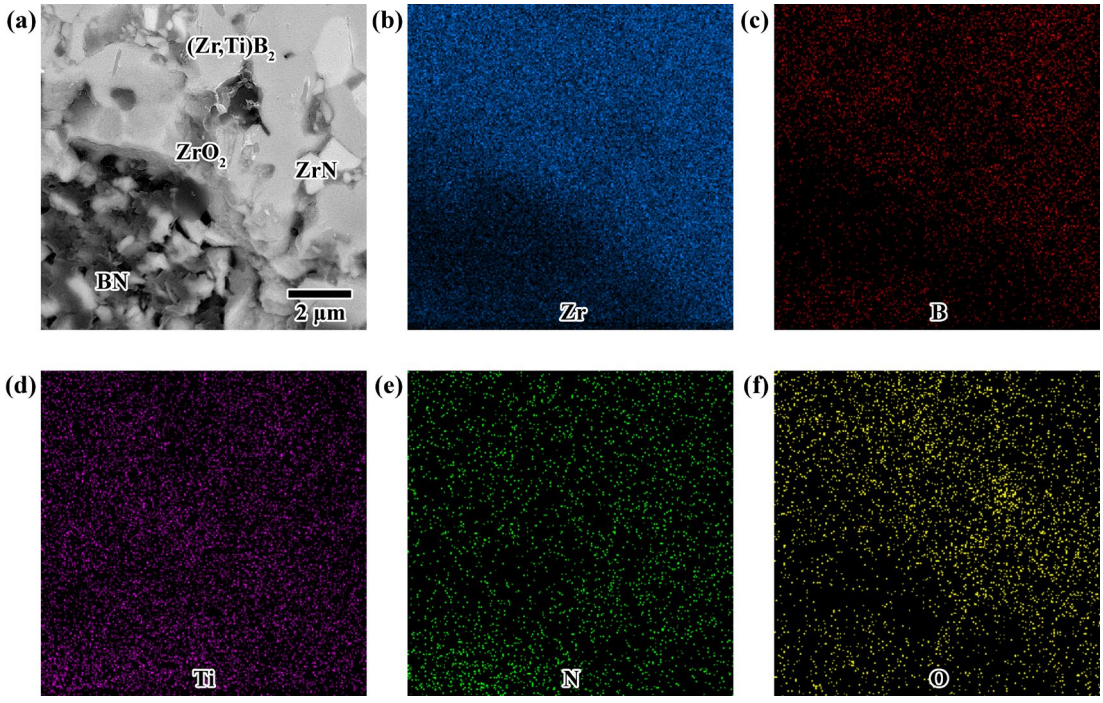

Fig. 2. Back scattered electron FE-SEM fractograph of ZT specimen and related EDS maps.

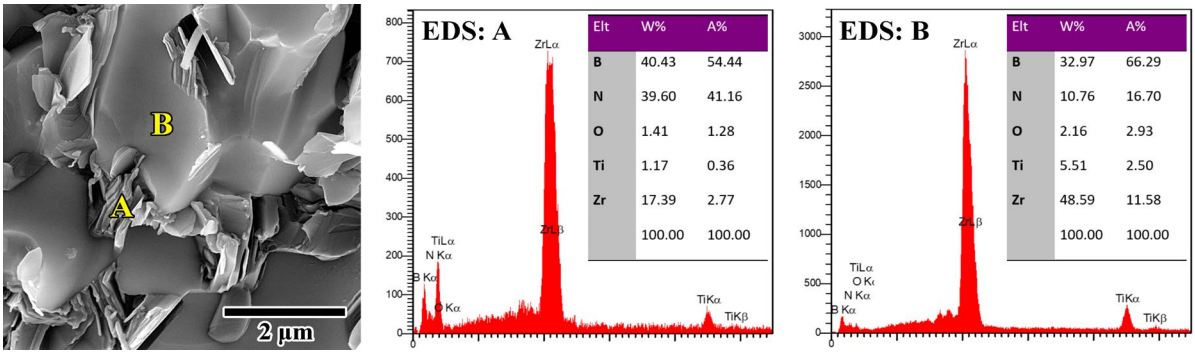

Fig. 3. FE-SEM fractograph of ZT sample and EDS analysis verifying h-BN formation.

fractured surface of ZT ceramic and its related EDS point spectra. According to the corresponding EDS spectra, the continuous matrix phase marked by 'B' in Fig. 3 has a high concentration of zirconium and boron elements, which seems to be ZrB_2 as the main phase. In addition, it had been discussed above that there is a possibility of $(Zr,Ti)B_2$ formation. Therefore, according to the related EDS analysis of point B, it seems that this point is the $(Zr,Ti)B_2$ solid solution. Also, EDS analysis of area 'A' (Fig. 3) shows that high-aspect-ratio phases surrounded among the matrix grains may be in-situ synthesized h-BN with platelet structure. Since there is no trace of titanium and nitrogen, the TiN additive seems to be totally consumed during the consolidation.

Identification of the crystalline phase composition of as-sintered Z and ZT samples was performed using XRD analysis. Fig. 4 exhibits the result of the XRD pattern of the ZT sample. As it was expected, the only phase recognized in the XRD pattern of the Z sample (not shown here) was ZrB_2. As can be seen in the phase composition of the ZT sample shown in Fig. 4, not only ZrB_2 is present as the main phase in the microstructure of TiN-doped material, but also some new phases including h-BN and ZrN are recognized as the in-situ formed phases. These new phases were synthesized during the spark plasma sintering process as a result of the introduction of 5 wt% TiN into the ZrB_2 matrix.

None of the phase analysis and microstructure observations could identify traces of TiN, which indicates that this sintering aid was probably completely consumed during the SPS processing. The following chemical reaction between ZrB_2 and TiN seems to be the reason for the disappearance of the TiN phase.

$$ZrB_2 + TiN = TiB_2 + ZrN \quad (2)$$

ZrN as a by-product of the aforesaid equation is the synthesized phase that is detected in the XRD pattern shown in Fig. 4. TiB_2 as another by-product of Eq. 2 is an essential compound to form the $(Zr,Ti)B_2$ solid solution. Zirconium nitride and mentioned solid solution form at the same time. In other words, nitrogen atoms must penetrate into the ZrB_2 structure and replace boron atoms to form ZrN. It will be possible when zirconium atoms of ZrB_2 can be replaced by titanium atoms and form the solid solution of $(Zr,Ti)B_2$. The lower melting point of the aforesaid solid solution compared to ZrB_2 reduces the temperature required for sintering and thus improves sinterability [45, 46]. Boria (B_2O_3) as a surface contamination on the particles of ZrB_2 can be reduced through a chemical reaction (Eq. 3) with in-situ synthesized ZrN obtained from the Eq. 2. ZrB_2 that is in-situ synthesized during the heating process develop microstructure and encourages the sinterability of the material owing to its

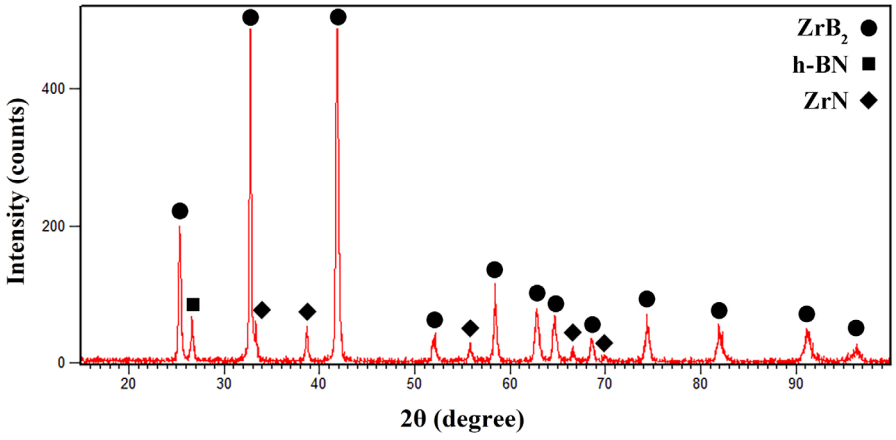

Fig. 4. XRD result of as-sintered ZT sample.

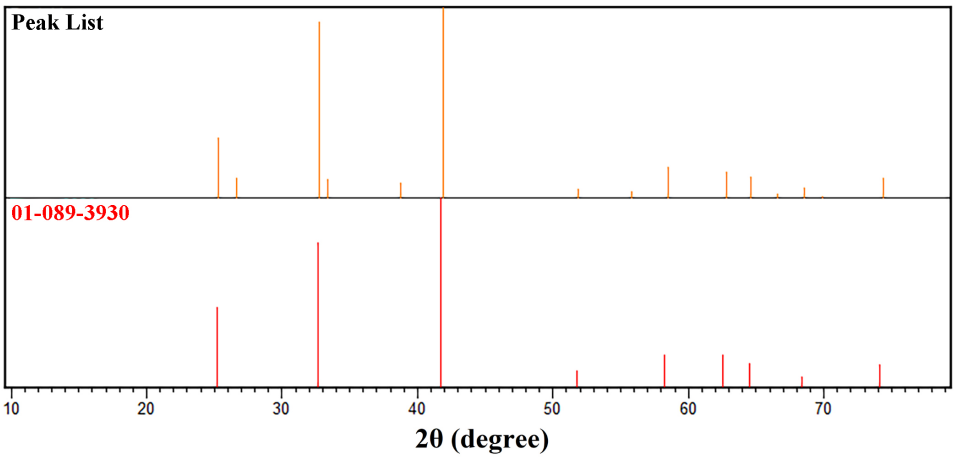

Fig. 5. Comparison of ZrB_2 peaks position of ZT sample with those in JCPDS card No. 01-089-3930.

ultra-fine size. The tendency of fine particles to bind to larger particles is lowering the energy level and increase stability. In order to reduce the energy level and increase the own stability, fine particles tend to connect to larger ones. According to Fig. 2, there are areas where the concentration of oxygen and zirconium is high, which indicates the presence of oxide impurities in the ZT sample. Based on the above statements and the formation of ZrO_2 as a by-product in Eq. 3, it seems that this oxide is present in the microstructure, but it has not been to the extent that it can be identified by XRD.

$$10ZrN + 6B_2O_3 = 9ZrO_2 + ZrB_2 + 10BN \quad (3)$$

Fig. 5 compares the ZrB_2 peak positions of the ZT sample with that those of standard JCPDS card (No. 01- 089-3930). On one hand, as it is clear from Fig. 5, there is a small peak shift towards a higher angle as 5 wt% TiN is added to ZrB_2. On the other hand, no phase including the titanium element is detected using analysis methods of XRD and EDS. These observations strengthen the theory of the solid solution formation of $(Zr,Ti)B_2$. Titanium with an atomic radius of 0.147 nm substitutes zirconium atoms with an atomic radius of 0.162 nm [47]. When smaller atoms substitute for larger ones, the structure of the host phase is subjected to compressive stress, which leads to a decrease in its lattice parameters. Based on Bragg's law, it is obvious that a shift in peaks towards a higher angle occurs with decreasing interfacial spacing due to the reduction of lattice parameters.

Fig. 6 illustrated the measured Vickers hardness for as-sintered ceramic materials. As seen in Fig. 6, the addition of a small amount of nitride component (5 wt% TiN) can promote the hardness by about 80%. Hardness is defined as a material's quality to resist localized plastic deformation (surface indentation). Since porosities do not show any resistance to applied forces, then materials with higher porosity show less hardness. Using the TiN additive not only encourages sinterability and densification of ZrB_2 material but also can improve the hardness. The increase in Vickers hardness is not only due to the densification improvement, another reason is the formation of new secondary phases that are inherently harder than initial materials. On the other hand, as is seen in Fig. 7, restricting the exceeding growth of grains through the synthesis of in-situ phases has also helped to improve hardness. It is clear from FE-SEM images from fractured sections of as-sintered samples shown in Fig. 7, adding 5 wt% TiN not only leads to the limitation of extreme growth of ZrB_2 grains but also results in the elimination of pores and porosities. It should be noted that according to the initial particle size of ZrB_2 (≤ 1.5 µm), hot pressing of pure ZrB_2 at 1800 °C under an external load of 15 MPa for 1 h caused the grains of ZrB_2 to grow excessively so that its grain size was measured to be around 15 µm (see Fig. 7a). It can be observed in Fig. 7, incorporation of only 5 wt% TiN into ZrB_2 has been able to minimize grain growth; hence, the mean size of ZrB_2 grains in this sample has decreased to 7 µm.

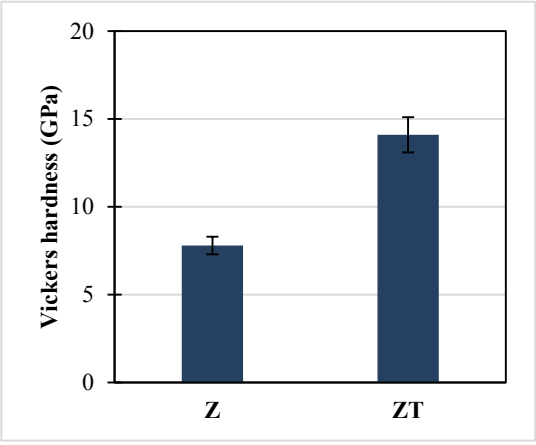

Fig. 6. Measured values of Vickers hardness of as-sintered samples.

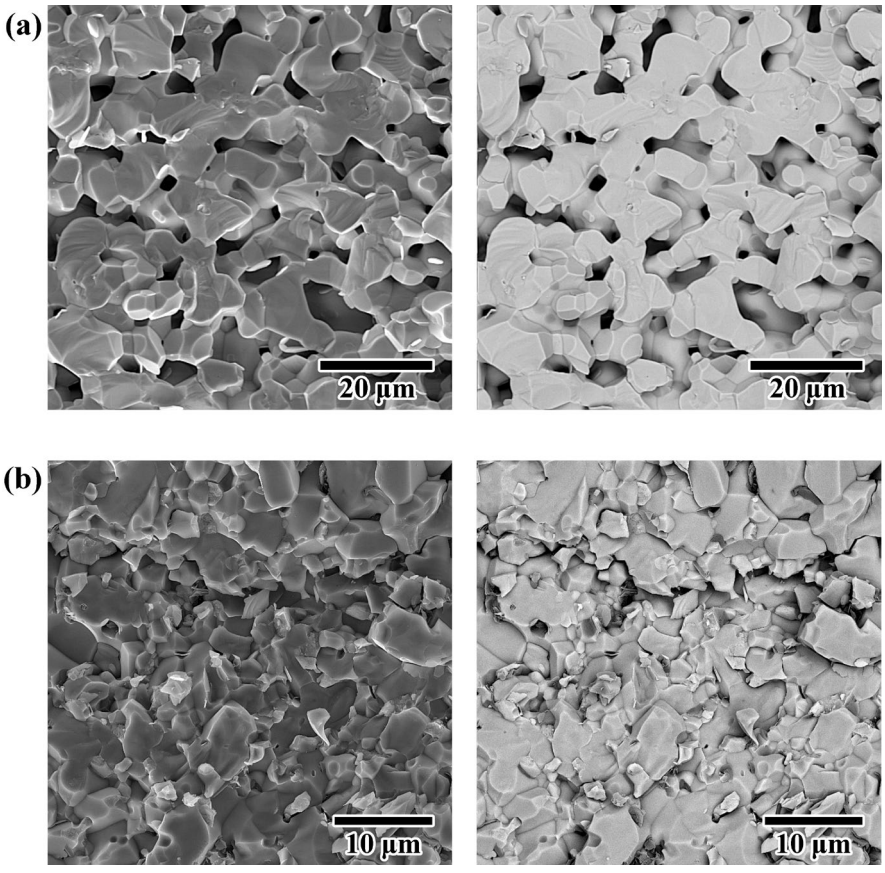

Fig. 7. FE-SEM images of fracture surfaces of as-sintered a) Z and b) ZT samples.

The measured values of fractured toughness are shown in Fig. 8. Improvement of fractured toughness can be seen from Fig. 8. It is clear that the addition of TiN additive has had a positive effect on these properties, so this feature has been promoted by about 2.5 times using 5 wt% TiN and fracture toughness of 3.8 MPa.m$^{1/2}$ was achieved. The fracture toughness of materials

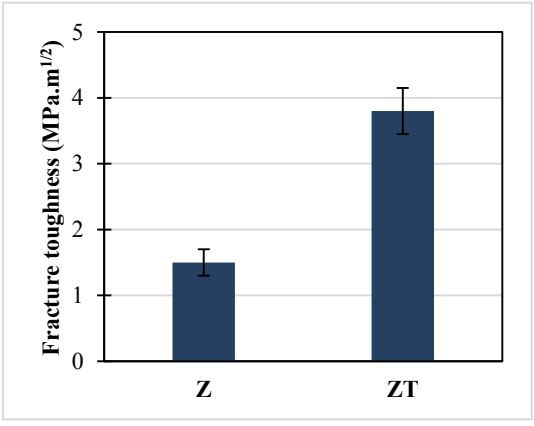

Fig. 8. Measured indentation fractures toughness of Z and ZT samples.

can be influenced by various factors. Relative density is one of the common factors affecting this property. Since adding TiN has led to densification promotion, it seems logical to increase toughness. Therefore, improving the densification during the sintering process of ceramics is very important, because it can affect the mechanical properties of these materials like hardness, fracture toughness, and strength. The fracture toughness of ZrB_2-based materials not only can be improved by densification but also can be influenced by their phase composition and microstructure.

The path of crack propagation caused by the Vickers indenter test performed on the polished surface of the as-sintered specimens is demonstrated in Fig. 9. As is observed in Fig. 9a, toughening mechanisms like bridging or toughening have not occurred in the Z sample during the crack spreading. It means that this sample shows low indentation fracture toughness. While, a small amount of TiN is added to ZrB_2 different types of toughening mechanisms such as grain breaking, crack deflection, bridging, and crack branching can be found in the microstructure of the ZT specimen. In-situ forming new phases like ZrN and h-BN assist to absorb the energy of cracks. It can be understood from Fig. 9b, on one hand, large ZrN grains are fractured as cracks reach them and as a result, it reduces their energy. On the other hand, h-BN with its soft structure and high aspect ratio can have an important role in observing the crack energy.

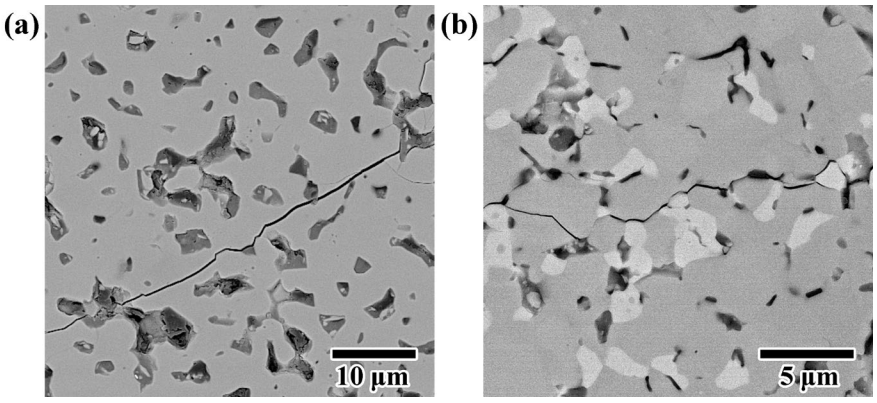

Fig. 9. The path of crack propagation in a) Z and b) ZT microstructures.

4. Conclusions

Influence of adding TiN as the sintering additive in ZrB_2 ceramic material was investigated. Therefore, the pure ZrB_2 and ZrB_2-5 wt% TiN were hot pressed for a dwell time of 60 min at a temperature of 1800 °C under a mechanical pressure of 15 MPa. The densification and sinterability of ZrB_2 ceramic importantly evolved when only small content of TiN (5 wt%) was introduced to this material. XRD and FE-SEM studies evidenced that new secondary phases like ZrN, $(Zr,Ti)B_2$ solid solution, h-BN, and ZrO_2 form through removing oxide impurities on the ZrB_2 particles' surface via chemical reactions. The grain size of ZrB_2 is minimized by the incorporation of TiN; thus, its mechanical features are improved so that the values of 14.1 GPa and 3.8 $MPa.m^{1/2}$ were attained for Vickers hardness and fracture toughness, respectively.

CRediT authorship contribution statement

Alain Shima: Conceptualization, Supervision, Writing – original draft. **Masoud Kazemi:** Investigation, Methodology, Writing – review & editing.

Data availability

The data underlying this article will be shared on reasonable request to the corresponding author.

Declaration of competing interest

The authors declare no competing interests.

Funding and acknowledgment

The authors would like to thank the University of Kyrenia and the Materials and Energy Research Center for their invaluable supports.

References

[1] A. Akbarpour, M. Sobhani, O. Mirzaee, M. Zakeri, Ablation resistance of graphite coated by spark plasma sintered ZrB2–SiC based composites, Bol. Soc. Esp. Ceram. Vidr. 61 (2022) 604–610. https://doi.org/10.1016/j.bsecv.2021.05.004.

[2] A. Chamberlain, W.G. Fahrenholtz, W.G. Fahrenholtz, D.T. Ellerby, High-Strength Zirconium Diboride-Based Ceramics, J. Am. Ceram. Soc. 87 (2004) 1170–1172. https://doi.org/10.1111/j.1551-2916.2004.01170.x.

[3] F. Sadegh Moghanlou, M. Vajdi, A. Motallebzadeh, J. Sha, M. Shokouhimehr, M. Shahedi Asl, Numerical analyses of heat transfer and thermal stress in a ZrB2 gas turbine stator blade, Ceram. Int. 45 (2019) 17742–17750. https://doi.org/10.1016/j.ceramint.2019.05.344.

[4] S. Mungiguerra, G.D. Di Martino, A. Cecere, R. Savino, L. Zoli, et al., Ultra-high-temperature testing of sintered ZrB2-based ceramic composites in atmospheric re-entry environment, Int. J. Heat Mass Transf. 156 (2020) 119910. https://doi.org/10.1016/j.ijheatmasstransfer.2020.119910.

[5] T. R. Paul, M.K. Mondal, M. Mallik, Densification behavior of ZrB2–MoSi2–SiCw composite processed by multi stage spark plasma sintering, Ceram. Int. 47 (2021) 31948–31972. https://doi.org/10.1016/j.ceramint.2021.08.081.

[6] S. Haghgooye Shafagh, S. Jafargholinejad, S. Javadian, Beneficial effect of low BN additive on densification and mechanical properties of hot-pressed ZrB2–SiC composites, Synth. Sinter. 1 (2021) 69–75. https://doi.org/10.53063/synsint.2021.1224.

[7] P. Vaziri, Z. Balak, Improved mechanical properties of ZrB2-30 vol% SiC using zirconium carbide additive, Int. J. Refract. Met. Hard Mater. 83 (2019) 104958. https://doi.org/10.1016/j.ijrmhm.2019.05.004.

[8] P. Sengupta, S.S. Sahoo, A. Bhattacharjee, S. Basu, I. Manna, Effect of TiC addition on structure and properties of spark plasma sintered ZrB2–SiC–TiC ultrahigh temperature ceramic composite, J. Alloys Compd. 850 (2021) 156668. https://doi.org/10.1016/j.jallcom.2020.156668.

[9] S. Jafari, M. Bavand-Vandchali, M. Mashhadi, A. Nemati, Effects of HfB2 addition on pressureless sintering behavior and microstructure of ZrB2-SiC composites, Int. J. Refract. Met. Hard Mater. 94 (2021) 105371. https://doi.org/10.1016/j.ijrmhm.2020.105371.

[10] S.D. Oguntuyi, O.T. Johnson, M.B. Shongwe, Spark Plasma Sintering of Ceramic Matrix Composite of ZrB2 and TiB2: Microstructure, Densification, and Mechanical Properties—A Review. Met. Mater. Int. 27 (2021) 2146–2159. https://doi.org/10.1007/s12540-020-00874-8.

[11] M. Saravana Kumar, S. Rashia Begum, M. Vasumathi, C.C. Nguyen, Q.V. Le, Influence of molybdenum content on the microstructure of spark plasma sintered titanium alloys, Synth. Sinter. 1 (2021) 41–47. https://doi.org/10.53063/synsint.2021.1114.

[12] E. Dodi, Z. Balak, H. Kafashan, HfB2-doped ZrB2-30 vol.% SiC composites: oxidation resistance behavior, Mater. Res. Express. 8 (2021) 045605. https://doi.org/10.1088/2053-1591/abdf1a.

[13] N.S. Peighambardoust, Ç. Çevik, T. Assar, S. Jung, S.Y. Lee, J. Hwan Cha, Pulsed electric current sintering of TiB2-based ceramics using nitride additives, Synth. Sinter. 1 (2021) 28–33. https://doi.org/10.53063/synsint.2021.1112.

[14] H. Wang, D. Chen, C.-A. Wang, R. Zhang, D. Fang, Preparation and characterization of high-toughness ZrB2/Mo composites by hot-pressing process, Int. J. Refract. Met. Hard Mater. 27 (2009) 1024–1026. https://doi.org/10.1016/j.ijrmhm.2009.06.003.
[15] M. Shahedi Asl, B. Nayebi, Z. Ahmadi, S. Parvizi, M. Shokouhimehr, A novel ZrB2–VB2–ZrC composite fabricated by reactive spark plasma sintering, Mater. Sci. Eng. A. 731 (2018) 131–139. https://doi.org/10.1016/j.msea.2018.06.008.
[16] S.K. Mishra, S.K. Das, A.K. Ray, P. Ramachandrarao, Effect of Fe and Cr Addition on the Sintering Behavior of ZrB2 Produced by Self-Propagating High-Temperature Synthesis, J. Am. Ceram. Soc. 85 (2002) 2846–2848. https://doi.org/10.1111/j.1151-2916.2002.tb00540.x.
[17] B. Mohammadpour, Z. Ahmadi, M. Shokouhimehr, M. Shahedi Asl, Spark plasma sintering of Al-doped ZrB2–SiC composite, Ceram. Int. 45 (2018) 4262–4267. https://doi.org/10.1016/j.ceramint.2018.11.098.
[18] J.J. Meléndez-Martínez, A. Domínguez-Rodríguez, F. Monteverde, C. Melandri, G. de Portu, Characterisation and high temperature mechanical properties of zirconium boride-based materials, J. Eur. Ceram. Soc. 22 (2002) 2543–2549. https://doi.org/10.1016/S0955-2219(02)00114-0.
[19] X. Sun, W. Han, Q. Liu, P. Hu, C. Hong, ZrB2-ceramic toughened by refractory metal Nb prepared by hot-pressing, Mater. Des. 31 (2010) 4427–4431. https://doi.org/10.1016/j.matdes.2010.04.020.
[20] E. Ghasali, M. Shahedi Asl, Microstructural development during spark plasma sintering of ZrB2–SiC–Ti composite, Ceram. Int. 44 (2018) 18078–18083. https://doi.org/10.1016/j.ceramint.2018.07.011.
[21] F. Monteverde, The thermal stability in air of hot-pressed diboride matrix composites for uses at ultra-high temperatures, Corros. Sci. 47 (2005) 2020–2033. https://doi.org/10.1016/j.corsci.2004.09.019.
[22] F. Monteverde, A. Bellosi, Development and characterization of metal-diboride-based composites toughened with ultra-fine SiC particulates, Solid State Sci. 7 (2005) 622–630. https://doi.org/10.1016/j.solidstatesciences.2005.02.007.
[23] F. Monteverde, A. Bellosi, Effect of the addition of silicon nitride on sintering behaviour and microstructure of zirconium diboride, Scr. Mater. 46 (2002) 223–228. https://doi.org/10.1016/S1359-6462(01)01229-5.
[24] Z. Ahmadi, B. Nayebi, M. Shahedi Asl, M. Ghassemi Kakroudi, I. Farahbakhsh, Sintering behavior of ZrB2–SiC composites doped with Si3N4: A fractographical approach, Ceram. Int. 43 (2017) 9699–9708. https://doi.org/10.1016/j.ceramint.2017.04.144.
[25] H. Wu, W. Zhang, Fabrication and properties of ZrB2–SiC–BN machinable ceramics, J. Eur. Ceram. 30 (2010) 1035–1042. https://doi.org/10.1016/j.jeurceramsoc.2009.09.022.
[26] G. Li, W. Han, B. Wang, Effect of BN grain size on microstructure and mechanical properties of the ZrB2–SiC–BN composites, Mater. Des. 32 (2011) 401–405. https://doi.org/10.1016/j.matdes.2010.05.051.
[27] M. Maleki, A. Beitollahi, J. Lee, M. Shokouhimehr, J. Javadpour, et al., One pot synthesis of mesoporous boron nitride using polystyrene-b-poly(ethylene oxide) block copolymer, RSC Adv. 5 (2015) 6528–6535. https://doi.org/10.1039/C4RA11431K.
[28] M. Maleki, M. Shokouhimehr, H. Karimian, A. Beitollahi, Three-dimensionally interconnected porous boron nitride foam derived from polymeric foams, RSC Adv. 6 (2016) 51426–51434. https://doi.org/10.1039/C6RA07751J.
[29] M. Maleki, A. Beitollahi, M. Shokouhimehr, Simple Synthesis of Two-Dimensional Micro/Mesoporous Boron Nitride, Eur. J. Inorg. Chem. 2015 (2015) 2478–2485. https://doi.org/10.1002/ejic.201500194.
[30] M. Maleki, A. Beitollahi, M. Shokouhimehr, Template-free synthesis of porous boron nitride using a single source precursor, RSC Adv. 5 (2015) 46823–46828. https://doi.org/10.1039/C5RA04636J.
[31] F. Shayesteh, S.A. Delbari, Z. Ahmadi, M. Shokouhimehr, M. Shahedi Asl, Influence of TiN dopant on microstructure of TiB2 ceramic sintered by spark plasma, Ceram. Int. 45 (2019) 5306–5311. https://doi.org/10.1016/j.ceramint.2018.11.228.
[32] W. Han, G. Li, X. Zhang, J. Han, Effect of AlN as sintering aid on hot-pressed ZrB2–SiC ceramic composite, J. Alloys Compd. 471 (2009) 488–491. https://doi.org/10.1016/j.jallcom.2008.03.135.
[33] Z. Ahmadi, B. Nayebi, M. Shahedi Asl, M. Ghassemi Kakroudi, Fractographical characterization of hot pressed and pressureless sintered AlN-doped ZrB2–SiC composites, Mater. Charact. 110 (2015) 77–85. https://doi.org/10.1016/j.matchar.2015.10.016.
[34] J.-H. Park, Y.H. Koh, H.E. Kim, C.S. Hwang, E.S. Kang, Densification and Mechanical Properties of Titanium Diboride with Silicon Nitride as a Sintering Aid, J. Am. Ceram. Soc. 82 (1999) 3037–3042. https://doi.org/10.1111/j.1151-2916.1999.tb02199.x.
[35] Z. Hamidzadeh Mahaseni, M. Dashti Germi, Z. Ahmadi, M. Shahedi Asl, Microstructural investigation of spark plasma sintered TiB2 ceramics with Si3N4 addition, Ceram. Int. 44 (2018) 13367–13372. https://doi.org/10.1016/j.ceramint.2018.04.171.
[36] M. Dashti Germi, Z. Hamidzadeh Mahaseni, Z. Ahmadi, M. Shahedi Asl, Phase evolution during spark plasma sintering of novel Si3N4-doped TiB2–SiC composite, Mater. Charact. 145 (2018) 225–232. https://doi.org/10.1016/j.matchar.2018.08.043.
[37] F. Monteverde, S. Guicciardi, A. Bellosi, Advances in microstructure and mechanical properties of zirconium diboride based ceramics, Mater. Sci. Eng. A. 346 (2003) 310–319. https://doi.org/10.1016/S0921-5093(02)00520-8.
[38] L.-H. Li, H.-E. Kim, E.S. Kang, Sintering and mechanical properties of titanium diboride with aluminum nitride as a sintering aid, J. Eur. Ceram. 22 (2002) 973–977. https://doi.org/10.1016/S0955-2219(01)00403-4.
[39] M. Shahedi Asl, S.A. Delbari, F. Shayesteh, Z. Ahmadi, A. Motallebzadeh, Reactive spark plasma sintering of TiB2–SiC–TiN novel composite, Int. J. Refract. Met. Hard Mater. 81 (2019) 119–126. https://doi.org/10.1016/j.ijrmhm.2019.02.022.
[40] C. Hu, Y. Sakka, H. Tanaka, T. Nishimura, S. Grasso, Synthesis, microstructure and mechanical properties of (Zr,Ti)B2-(Zr,Ti)N composites prepared by spark plasma sintering, J. Alloys Compd. 494 (2010) 266–270. https://doi.org/10.1016/j.jallcom.2010.01.006.
[41] Z. Ahmadi, M. Zakeri, M. Farvizi, A. Habibi-Yangjeh, S. Asadzadeh-Khaneghah, M. Shahedi Asl, Synergistic influence of SiC and C3N4 reinforcements on the characteristics of ZrB2-based composites, J. Asian Ceram. Soc. 9 (2021) 53–62. https://doi.org/10.1080/21870764.2020.1847425.
[42] G.R. Anstis, P. Chantikul, B.R. Lawn, D.B. Marshall, A Critical Evaluation of Indentation Techniques for Measuring Fracture Toughness: I, Direct Crack Measurements, J. Am. Ceram. Soc. 64 (1981) 533–538. https://doi.org/10.1111/j.1151-2916.1981.tb10320.x.
[43] Z. Ahmadi, M. Shahedi Asl, M. Zakeri, M. Farvizi, Fabrication of (Zr,Ti)B2–ZrN–BN composites through reactive spark plasma sintering of ZrB2 and TiN, Micron. 154 (2022) 103203. https://doi.org/10.1016/j.micron.2021.103203.
[44] Z. Ahmadi, M. Shahedi Asl, M. Zakeri, M. Farvizi, On the reactive spark plasma sinterability of ZrB2–SiC–TiN composite, J. Alloys Compd. 909 (2022) 164611. https://doi.org/10.1016/j.jallcom.2022.164611.
[45] J. Li, J. Han, S. Meng, B. Wang, Valence electron structure of the (ZrTi)B2 solid solutions calculated by the three models, Sci. China Ser. E: Technol. Sci. 52 (2009) 1195–1201. https://doi.org/10.1007/s11431-009-0011-x.
[46] W.M. Wang, H. Wang, Z.Y. Fu, Microstructure and Mechanical Properties of the Boride Doping TiB2 Ceramic, Key Eng. Mater. 249 (2003) 109–114. https://doi.org/10.4028/www.scientific.net/KEM.249.109.
[47] B. Fu, H. Wang, C. Zou, Z. Wei, The influence of Zr content on microstructure and precipitation of silicide in as-cast near α titanium alloys, Mater. Charact. 99 (2015) 17–24. https://doi.org/10.1016/j.matchar.2014.09.015.